Design and Experimental Analysis of PFC Rectifiers for Domestic Induction Heating Applications

Mario Pérez-Tarragona, *Student Member, IEEE*, Héctor Sarnago, *Member, IEEE*, Óscar Lucía, *Senior Member, IEEE*, and José M. Burdío, *Senior Member, IEEE*

***Abstract*—Induction heating is nowadays a key technology due to its advantages in terms of performance and efficiency, which has boosted its adoption in industrial, domestic, and medical applications, among others. Recent developments in domestic induction heating are focused on flexible cooking surfaces with higher output power. The design requirements of this cooktops are more restrictive due to electromagnetic compatibility (EMC), power density, efficiency, control complexity, and cost. In order to overcome these issues, the use of active power factor corrector (PFC) rectifiers is proposed. This paper proposes and analyzes a complete set of modulation strategies for a single-phase boost-type PFC applied to domestic induction heating. A comparative analysis is performed taking into account the device stress, efficiency, operating frequency, control complexity, and EMC performance. This discussion reveals the advantages and disadvantages of each modulation strategy according to the final implementation requirements and the application area.**

***Index Terms*—Home appliances, induction heating (IH), modulation strategies, power factor corrector (PFC), resonant power conversion, zero voltage switching (ZVS).**

I. Introduction

IN THE last years, trends in domestic induction heating (IH) cooktops have led to bigger and more flexible cooking areas enabling the user using a wide variety of cooking utensils [1]. With this purpose, flexible cooking surfaces [2] with bigger coils with several concentric windings were proposed [see Fig. 1(a)]. More recently, flexible cooking surfaces with fully active surfaces appeared [see Fig. 1(b)], taking advantage of small-diameter coils distributed along the whole surface. It allows us virtually using any pan or pot, no matter the size or the shape [3]–[8].

The design requirements of the flexible cooking surfaces are usually more restrictive in terms of higher efficiency, due to environmental concerns and temperature limitations, higher output power, to supply the bigger IH loads, higher power density, due to space limitations, improved electromagnetic compatibility (EMC) performance, and low cost. In order to face these challenges and decrease the total implementation cost, it is desirable to use power factor corrector (PFC) rectifiers. A front-end PFC rectifier decreases the complexity of power electronics design because it allows us separating the EMC issues from the IH design. Besides, it allows us obtaining a common dc-bus that enables reducing the device ratings. A multiphase approach using multiphase rectifier is also interesting, since it allows us delivering higher output power compared with current state-of-the-art implementations. Consequently, this paper proposes and studies the use of a PFC converter to improve the user performance of modern IH appliances.

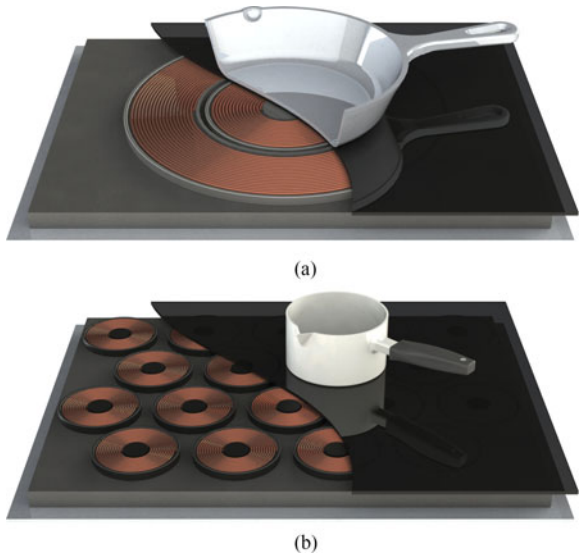

Fig. 1. Flexible cooking surfaces. (a) Classical concentric coils. (b) Fully active surface.

The PFC rectifiers are widely used in many applications and can be classified mainly in passive systems or active PFC systems [9], [10]. Passive PFC rectifiers do not need control elements. However, larger magnetic components are usually required for filtering and they are not able to reach current harmonic distortion, total harmonic distortion $(\mathrm{THD})_i$, smaller than 30% due to the large amount of low frequency harmonic components. For this reason, to fulfil the EMC standards [11] required for IH appliances, it is proposed to use active PFC rectifiers, since they can reach THD_i smaller than 3% and a high power density at the cost of a more complex control.

Manuscript received July 20, 2017; accepted September 13, 2017. Date of publication September 20, 2017; date of current version April 20, 2018. This work was supported in part by the Spanish MINECO under Project TEC2016-78358-R and Project RTC-2014-1847-6, in part by the Spanish MECD under the FPU Grant FPU15/01590, in part by the DGA-FSE, and in part by the BSH Home Appliances Group. Recommended for publication by Associate Editor Francisco Javier Azcondo. *(Corresponding Author: Mario Pérez-Tarragona.)*

The authors are with the Department of Electronic Engineering and Communications, University of Zaragoza, Zaragoza 50018, Spain (e-mail: maperta@unizar.es; hsarnago@unizar.es; olucia@ieee.org; burdio@unizar.es).

Color versions of one or more of the figures in this paper are available online at http://ieeexplore.ieee.org.

Digital Object Identifier 10.1109/TPEL.2017.2755367

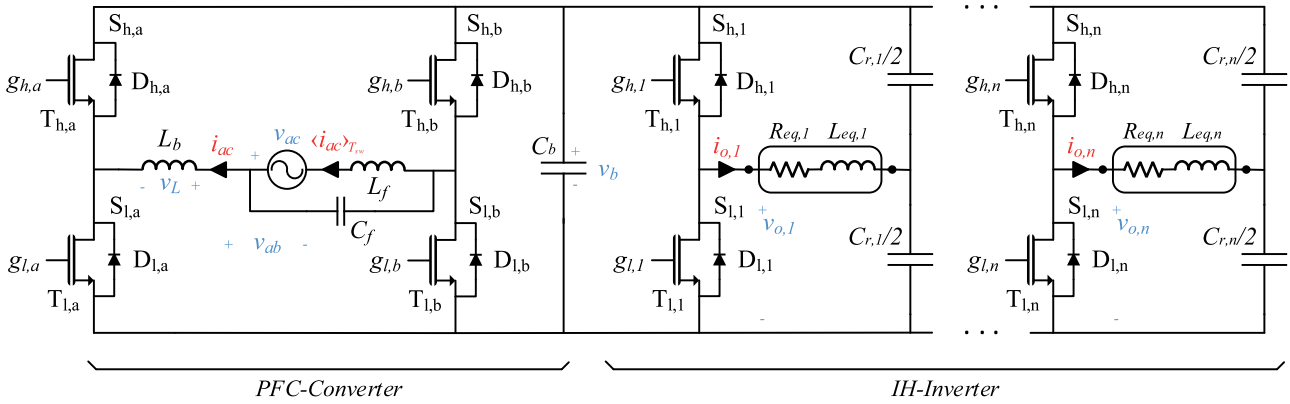

Fig. 2. Proposed PFC IH converter with *n* IH-loads.

Nowadays, PFC rectifiers have rarely been implemented in commercial IH home appliances due to complexity and cost issues [12], [13]. However, advances in power electronics and control, as well as the trend towards higher performance appliances motivates the proposed approach. Different topologies have been proposed that can perform this function, which can mainly be classified in buck-type converters and boost-type converters [10]. The latter are especially interesting in the IH field because allow us improving the efficiency in the downstream IH inverter.

In order to perform the PFC strategy, different modulations can be implemented [14]–[23]. However, each one of these strategies has some advantages and disadvantages that can encourage or complicate its implementation according to the application area, the control complexity, the cost, the device ratings, the efficiency, the EMC issues, or the operating frequency. Consequently, this paper proposes a detailed analysis of these modulation strategies and introduces new approaches with the aim of finding a good balance between cost, efficiency, and power density to obtain an effective implementation.

This paper is organized as follows. Section II presents the single-phase PFC IH converter topology used to implement every proposed modulation strategy, which are also analyzed and detailed. Section III introduces the control implementation. In Section IV, the main experimental results are shown. A discussion with a comparative analysis is performed taking into account the device stress, the efficiency, the control complexity, and the EMC issues. Finally, a domestic IH application is implemented using one of the proposed modulation strategies. Section V summarizes the main conclusions of this paper.

II. Proposed Topology and Modulation Strategies

The analysis of the modulation strategies has been performed using a single-phase PFC IH converter. In this section, the proposed topology is presented and the set of modulation strategies are detailed and analyzed.

A. Topology

The proposed PFC converter is shown in Fig. 2. It is based on the boost converter and it is composed of two half-bridge legs, *a* and *b*, which allow us short-circuiting the boost inductance, L_b, with the mains voltage, v_{ac}, with a period T_{ac}, and/or the bus voltage, v_b. Each half-bridge is composed of two switching devices, S_h and S_l, with MOSFETs, T_h and T_l, and antiparallel diodes, D_h and D_l. A filter between the mains and the PFC stage is placed, supplying the medium frequency currents and removing the high ripple of the boost coil current, i_{ac}. In this way, a fully filtered input current, $\langle i_{ac}\rangle_{T_{sw}}$, is achieved in the switching period $T_{sw} \ll T_{ac}$. In the proposed implementation, an inductance, L_f, and a capacitor, C_f, of filtering is used. A capacitor, C_b, filters the bus voltage, which powers the IH-inverter. The set is composed of as many half-bridge branches, $S_{h,n}$ and $S_{l,n}$, as IH-loads. Each IH-load is composed of the series equivalent resistance, $R_{\mathrm{eq},n}$, and inductance, $L_{\mathrm{eq},n}$, and the split resonant capacitor, $C_{r,n}$.

This converter allows us performing and analyzing each possible PFC modulation strategy according to the conduction mode: continuous conduction mode (CCM) or discontinuous conduction mode (DCM), the switching frequency (fixed or variable), and the switching mode (zero voltage switching, ZVS, or hard switching). Fig. 3 shows a classification of these modulation strategies according to the topology configuration: half bridge, full bridge, or a combination of both, i.e., hybrid. Each modulation strategy defines a different i_{ac} current.

1) Half Bridge: In half-bridge configuration, the *a* branch is activated at T_{sw}, while the *b* branch is activated at T_{ac} to get synchronous rectification. The main advantage of this configuration is that the switching device count is reduced. However, the main disadvantage is that the i_{ac} current control close to the mains-voltage zero-crossing becomes difficult. In this case, the mains voltage is null ($v_{ac} = 0$) while the bus capacitor is fully charged, leading to extreme duty cycles, and zero-crossing distortion when the duty cycle is limited. Fig. 3 shows the i_{ac} current and v_{ab} voltage waveforms. The duty cycle, *d*, using a CCM conduction mode depends on the mains voltage sign as follows:

$$d = \frac{v_{ac}}{v_b}, v_{ac} > 0$$
$$d = 1 + \frac{v_{ac}}{v_b}, v_{ac} < 0. \quad (1)$$

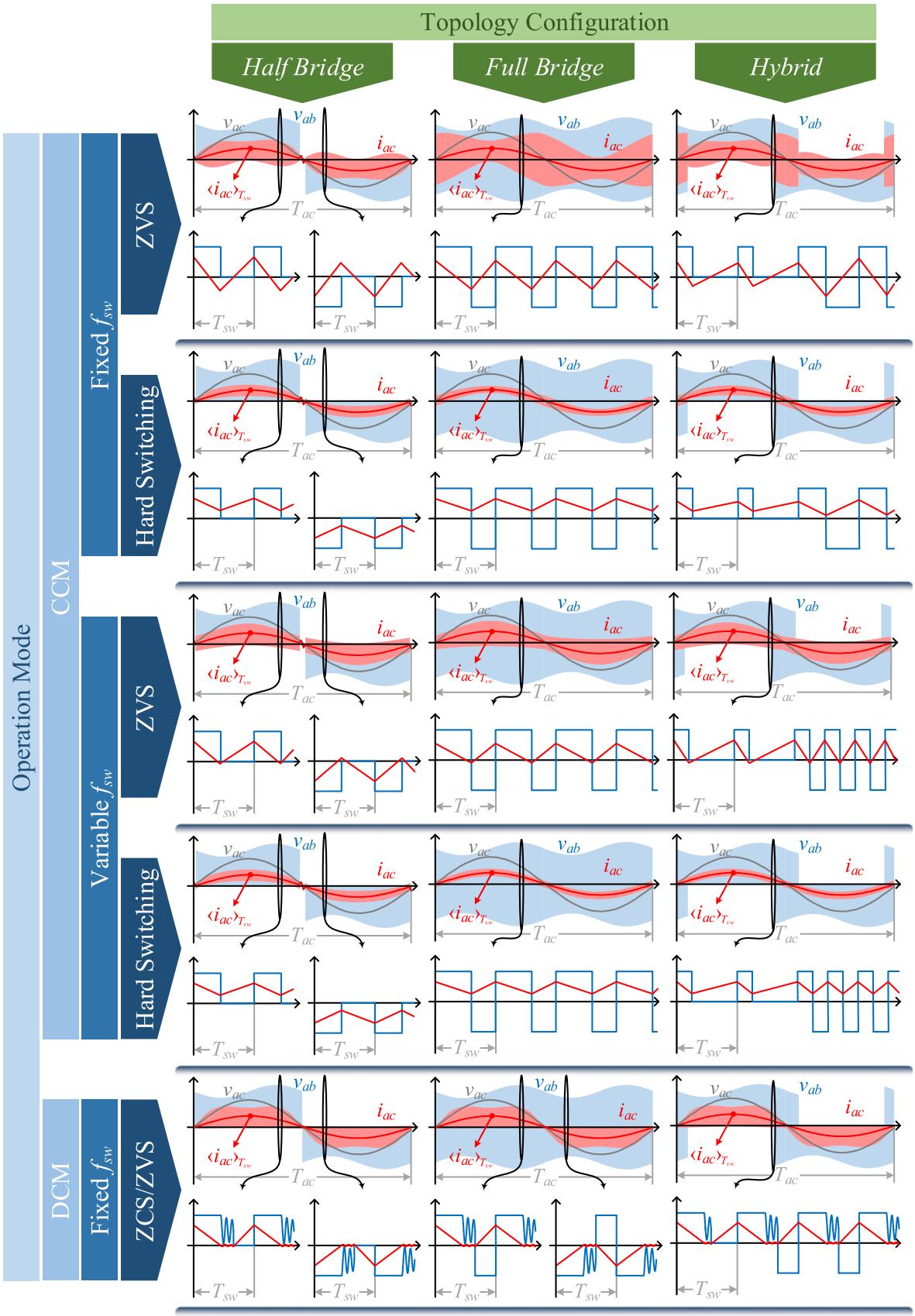

Fig. 3. Classification of the proposed modulation strategies depending on the topology configuration: half bridge, full bridge, or hybrid; and the operation mode: CCM or DCM with fixed or variable switching frequency, f_{sw}, and ZVS or hard switching.

2) Full Bridge: The second approach is based on using the two inverter branches phase-shifted 180° and complementary duty cycles. In this way, both branches are activated at T_{sw}. The main advantage of this strategy is that zero-cross distortion is avoided. However, the number of switching devices required is higher, increasing switching losses. Besides, voltage applied to the boost inductor is also higher, increasing the current ripple, and therefore conduction losses in the boost inductor and the switching devices. As a consequence, this approach leads to lower efficiency results.

In this case, the duty cycle does not depend on the mains voltage sign and its values are less extreme than in the half-bridge modulation, being 0.5 in the mains voltage zero crossing $(v_{ac} = 0)$ and easing the control. For each branch, the duty cycle in a CCM conduction mode is defined as

$$d_a = \frac{1}{2}\left(1 + \frac{v_{ac}}{v_b}\right)$$
$$d_b = \frac{1}{2}\left(1 - \frac{v_{ac}}{v_b}\right). \tag{2}$$

3) Hybrid: In order to improve both the efficiency and the zero-cross distortion, a combined approach is proposed. It consists in using the half-bridge configuration and changing to the full-bridge configuration close to the zero crossing. In this way, the distortion is eliminated at the cost of additional control complexity, but getting an improved efficiency in tradeoff with the full-bridge configuration. The combination of the two configurations decreases slightly the efficiency in comparison with the half-bridge configuration. However, it avoids the zero-cross distortion, achieving a good balance between efficiency and EMC performance.

B. Operation Modes

The CCM strategy can operate with fixed or variable frequency during the mains cycle. This operation mode with fixed frequency can be very interesting in applications that cannot modify the operating frequency. Besides, it can operate either with ZVS or hard switching. On the one hand, the main advantage of the ZVS operation is that the turn-ON switching losses are null, decreasing switching losses. However, the boost-inductor root mean square (RMS) current is increased due to the high ripple required to achieve the ZVS soft-switching behavior, increasing conduction losses in the boost coil and switching devices.

On the other hand, a reduced ripple current can be achieved by using a high inductance value, yielding to a hard-switching behavior. As an advantage, the RMS boost inductance current is reduced, improving conduction losses. Moreover, the filtering requirements are lower than with ZVS conditions due to the low ripple. In contrast, the efficiency levels can be decreased by the additional switching losses.

Finally, the DCM operation introduces an extra state in which all devices are deactivated, getting a null boost inductance voltage, v_L, and current, i_{ac}. This extra state allows us avoiding the zero-cross distortion in half-bridge configuration too. The antiparallel diodes are in charge of shorting the boost inductance current, i_{ac}, when it changes its polarity.

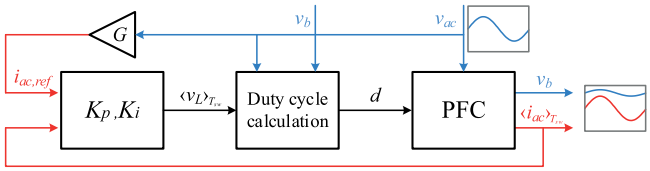

Fig. 4. Control scheme of the boost-inductor voltage control where the calculated action is the boost inductance voltage, v_L, which is used to calculate later the duty cycle, d, by using the converter parameters.

This conduction mode has the same drawbacks as the ZVS CCM since it also operates with a high current ripple. Moreover, the turn-ON switching losses are also null because of ZVS and ZCS switching.

III. Control Implementation

The proposed modulation strategies achieve different performance and cost figures of merit, as it has been previously analyzed. Besides, it is important to note that from an implementation point of view, the design of the control loop is different for each one. This section details the proposed control implementation strategies, which can be classified into four groups: boost-inductor voltage control, variable-frequency activation control, current mode control, and fixed-frequency activation control.

A. Boost-Inductor Voltage Control

The boost-inductor voltage control allows us performing all fixed frequency CCM strategies. The converter control consists in generating a sinusoidal reference current, $i_{ac,\mathrm{ref}}$, in phase with the mains voltage and with the desired RMS current value, $I_{ac,rms}$. The regulator adjusts the mains current, $\langle i_{ac} \rangle_{T_{sw}}$, to follow the reference exactly.

In order to control the system and to eliminate the stationary error, a proportional, K_p, and integral, K_i, regulator is proposed. In typical control schemes, the action calculated by the regulator is the duty cycle, d, applied to the PFC stage. However, this system is difficult to control using this scheme because its nonlinearity, which depends strongly on the mains voltage, the bus voltage, and the induction load.

To overcome this issue, using the boost coil local average voltage, $\langle v_L \rangle_{T_{sw}}$, as controller output action is proposed, as it is shown in Fig. 4. When the local average voltage in an inductance differs from zero, it means a variation of its average current. According to the differential equation that models the boost coil behavior

$$i_{ac}|_{t_0+T_{sw}} = i_{ac}|_{t_0} + \frac{1}{L_b}\int_{t_0}^{t_0+T_{sw}} v_L\, dt. \tag{3}$$

Consequently, the v_L voltage makes possible to control the boost-inductor average current, $\langle i_{ac} \rangle_{T_{sw}}$, linearly and therefore, the mains current can be properly shaped. Keeping in mind that the half-bridge or full-bridge configurations can be implemented, the duty cycle can be calculated in a second step with

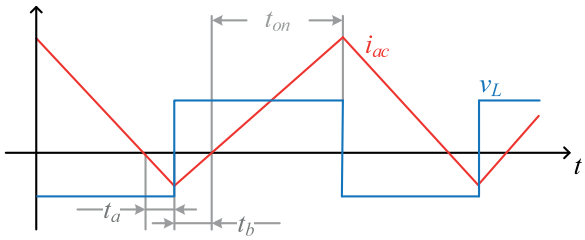

Fig. 5. Control scheme of the variable-frequency activation control. The activation time, t_{on}, the negative time, t_a, and the recovery time, t_b, are indicated along with the boost inductance current, i_{ac}, and voltage, v_L, waveforms.

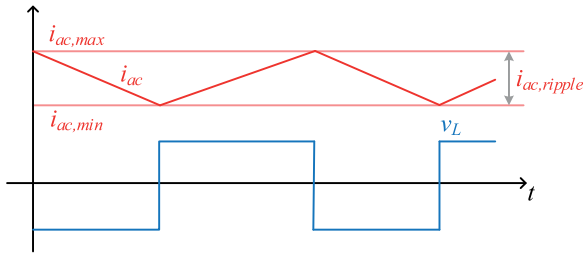

Fig. 6. Control scheme of the current mode control. The current ripple, $i_{ac,ripple}$, and the superior, $i_{ac,max}$, and inferior, $i_{ac,min}$, current limits are indicated along with the boost inductance current, i_{ac}, and voltage, v_L, waveforms.

(4) or (5), respectively

$$d = \frac{v_{ac} - v_L}{v_b}, v_{ac} > 0$$
$$d = 1 + \frac{v_{ac} - v_L}{v_b}, v_{ac} < 0. \quad (4)$$
$$d_a = \frac{v_{ac} + v_b - v_L}{2v_b}$$
$$d_b = 1 - d_a \quad (5)$$

where v_{ac} and v_b are the mains and the bus average voltage in a switching cycle, respectively.

In order to perform this control, the input voltage, v_{ac}, the input current, $\langle i_{ac} \rangle_{T_{sw}}$, and the bus voltage, v_b, have to be measured. The reference current, $i_{ac,\mathrm{ref}}$, is obtained by the product of the mains voltage, v_{ac}, and the transconductance, G. This parameter is defined from the RMS mains voltage, $V_{ac,rms}$, and the desired input power, P_{in}, as

$$G = \frac{P_{\mathrm{in}}}{V_{ac,rms}^2}. \quad (6)$$

B. Variable-Frequency Activation Control

With this control it is possible to perform the ZVS and variable frequency CCM strategy or, as it is also known, the critical CCM. It consists in stablishing an activation time, t_{on}, that defines the RMS input current value, $I_{ac,rms}$. To do this, the zero crossing of the boost inductance current, i_{ac}, has to be detected. Besides, a negative conduction or ZVS time, t_a, is defined in order to ensure the ZVS switching.

As it is shown in Fig. 5, first, a negative voltage is applied over the boost inductance. The moment in which the current turns on negative, the negative conduction, t_a, time is stablished. After that the devices switch to apply a positive voltage over the inductance. Later, the time that the current takes to turn ON positive is measured. This time is called recovery time, t_b, and is used to compensate the negative conduction time. Finally, the activation time, t_{on}, is applied and, after that, the devices switch to apply a negative voltage over the boost inductance again.

The voltage applied to the boost coil depends on the topology configuration, the mains voltage, v_{ac}, the bus voltage, v_b, and the switching device activation state. The negative conduction time affects to the operating frequency range and the current ripple, and can be chosen arbitrarily since it does not modify the desired RMS input current. It is just defined by the activation time, t_{on}, as a function of the recovery time, t_b, the mains voltage, v_{ac}, the bus voltage, v_b, the transconductance, G, and the boost inductance, L_b. The activation time is calculated with (7) or (8) according to the topology configuration: half bridge or full bridge, respectively. As it is shown by (7), in the half-bridge configuration the activation time is just defined by the recovery time, the transconductance, and the boost inductor, therefore, the mains and bus voltage do not need to be measured

$$t_{on} = 2L_bG + t_b \quad (7)$$
$$t_{on} = 2L_bG\left(\frac{v_{ac}}{v_b + v_{ac}}\right) + t_b. \quad (8)$$

C. Current Mode Control

In order to perform the hard switching and variable frequency CCM, a current mode control has been implemented. This control consists in stablishing a superior and inferior boost inductance current limit, $i_{ac,max}$ and $i_{ac,min}$, respectively. These limits depend on the reference current, $i_{ac,rms}$, and the desired current ripple, $i_{ac,ripple}$, as

$$i_{ac,max} = i_{ac,\mathrm{ref}} + \frac{i_{ac,ripple}}{2}$$
$$i_{ac,min} = i_{ac,\mathrm{ref}} - \frac{i_{ac,ripple}}{2}. \quad (9)$$

As in the boost-inductor voltage control, a sinusoidal reference current, $i_{ac,\mathrm{ref}}$, is generated in phase with the mains voltage and with the desired RMS current value, $I_{ac,rms}$, which is defined with the transconductance, G, as a function of the desired input power, P_{in}. The boost inductance current, i_{ac}, is measured with a current sensor. As it is shown in Fig. 6, the moment that the boost inductance current reaches the superior limit, $i_{ac,max}$, the switching devices switch in order to apply a negative voltage over the boost inductance and vice versa. When the boost inductance current reaches the inferior limit, $i_{ac,min}$, a positive voltage is applied over the boost inductance. The switching devices that are activated or deactivated to apply a positive or negative voltage over the boost inductance depend on the topology configuration. The switching frequency depends on the boost inductance, L_b, and the current ripple, $i_{ac,ripple}$.

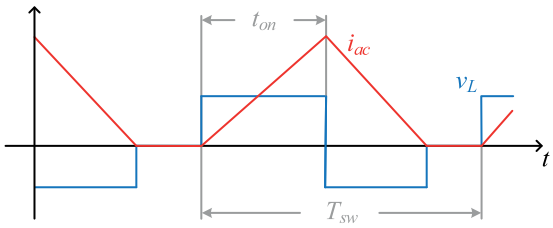

Fig. 7. Control scheme of the fixed-frequency activation control. The activation time, t_{on}, and the boost inductance current, i_{ac}, and voltage, v_L, waveforms are indicated.

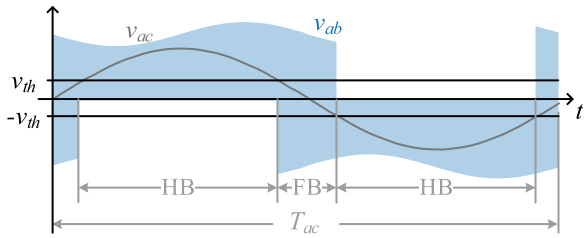

Fig. 8. Detail of the hybrid modulation control with the change voltage, v_{th}, indication.

D. Fixed-Frequency Activation Control

Finally, the fixed-frequency activation control has been implemented to perform the DCM strategy. It is similar to the variable-frequency activation control. However, in this case the current zero crossing does not need to be detected because the frequency is fixed and the activation time, t_{on}, is calculated as a function of the converter parameters and the switching period, T_{sw}, in order to achieve the extra state of DCM. The (10) and (11) allow us calculating this parameter using the half-bridge or full-bridge configuration, respectively. On both cases, the bus voltage, v_b, and the mains voltage, v_{ac}, have to be measured

$$t_{on} = \sqrt{2T_{sw}L_bG\frac{v_b - |v_{ac}|}{v_b}} \tag{10}$$

$$t_{on} = \sqrt{T_{sw}L_bG\frac{(v_b - v_{ac})\,v_{ac}}{(v_b + v_{ac})\,v_b}}. \tag{11}$$

Moreover, the negative conduction time, t_a, and the recovery time, t_b, are not necessary any more as it is shown in Fig. 7. The minimum switching period, $T_{sw,min}$, that allows us operating in DCM is calculated using (12) and (13) according to the topology configuration, half bridge or full bridge, respectively. It depends on the boost inductance, L_b, the transconductance, G, the bus voltage, v_b, and the mains voltage, v_{ac}. A conservative approach is based on considering the minimum bus voltage and the maximum mains voltage, i.e., $\sqrt{2}V_{ac,rms}$

$$T_{sw,min} = 2L_bG\frac{v_b}{v_b - v_{ac}} \tag{12}$$

$$T_{sw,min} = 4L_bG\frac{v_b v_{ac}}{v_b^2 - v_{ac}^2}. \tag{13}$$

Even though the control parameters depend on the topology configuration, the control strategy is independent. It allows us performing hybrid modulations using the same control strategy. The hybrid modulation consists in using usually the half-bridge configuration and the full-bridge configuration only when the bus voltage is close to zero to avoid the zero-cross distortion. In this way, the change voltage, v_{th}, parameter is defined. As it is shown in Fig. 8, when the absolute value of the mains voltage, $|v_{ac}|$, is higher than the change voltage, v_{th}, the half-bridge configuration is used.

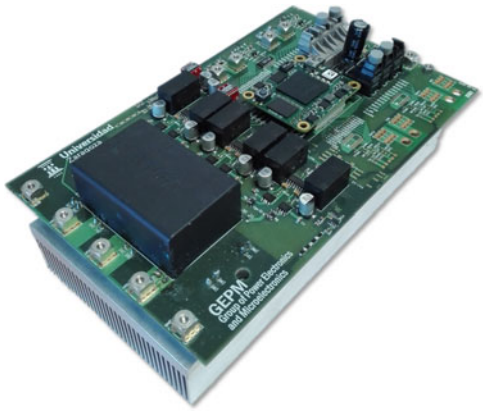

Fig. 9. Prototype used to implement the proposed strategies.

TABLE I
CONVERTER DESIGN PARAMETERS

Parameter	Value
Mains voltage, $V_{ac,rms}$	230 V RMS, 50 Hz
Input power range, P_{in}	500–3680 W
Bus voltage, v_b	400 V
Operating frequency, f_{sw}	40-180 kHz
Filter capacitor, C_f	5 μF
Filter coil, L_f	50 μH (Hard switching) 215 μH (ZVS)
Bus capacitor, C_b	1140 μF
Boost inductor, L_b	215 μH (Hard switching) 26 μH (ZVS)

IV. EXPERIMENTAL RESULTS AND DISCUSSION

A. Experimental Results

In order to perform and analyze each proposed strategy, a versatile platform has been designed and implemented. The prototype, shown in Fig. 9, is composed of a three-half-bridges module using CREE SiC MOSFETs. A Spartan-6 FPGA from Xilins is used to implement the control architecture. Besides, the whole system can be managed from the personal computer (PC) through a Wi-Fi module and a PC application has been developed using Visual Basic. The platform allows us measuring current using magneto-resistive current sensors and voltage using voltage dividers. Table I summarizes the main converter design parameters.

Fig. 10 shows the experimental results obtained using every modulation strategy with half-bridge or full-bridge configuration. For each modulation strategy, the main waveforms in a mains cycle are shown along with a zoomed detail. Moreover,

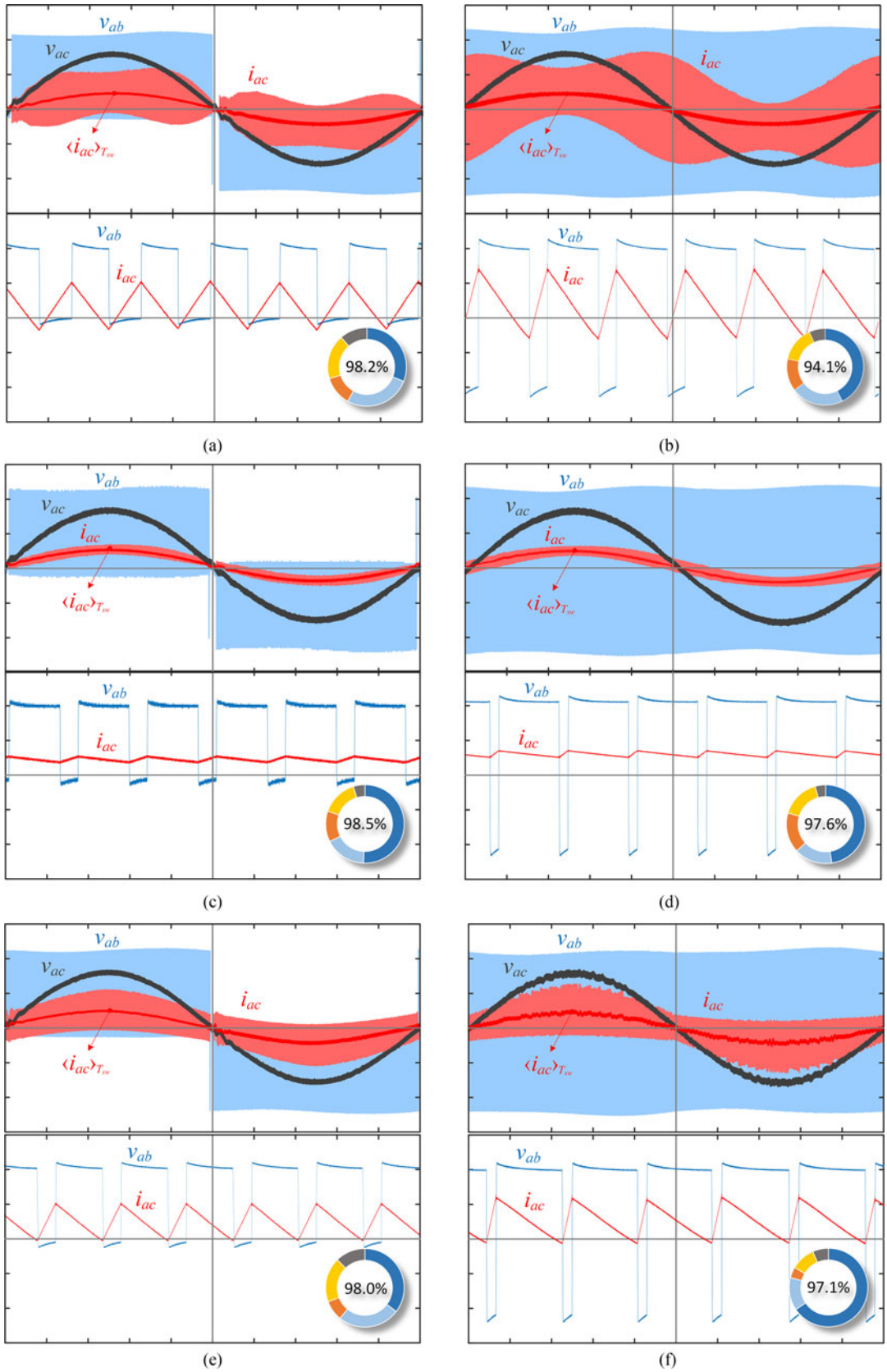

Fig. 10. ZVS, (a) and (b), or hard switching, (c) and (d), fixed frequency CCM, the ZVS, (e) and (f), or hard switching, (g) and (h), variable frequency CCM, and the ZVS/ZCS fixed frequency DCM, (i) and (j), modulation strategies. The half-bridge configuration on the left and the full-bridge configuration on the right. On the top, the main experimental waveforms (voltage: 200 V/div, current: 50 A/div, and time: 2 ms/div). On the bottom, a zoomed detail (time: 10 μs/div). In the lower right corner, the overall efficiency and the power loss distribution at maximum power, 3680 W.

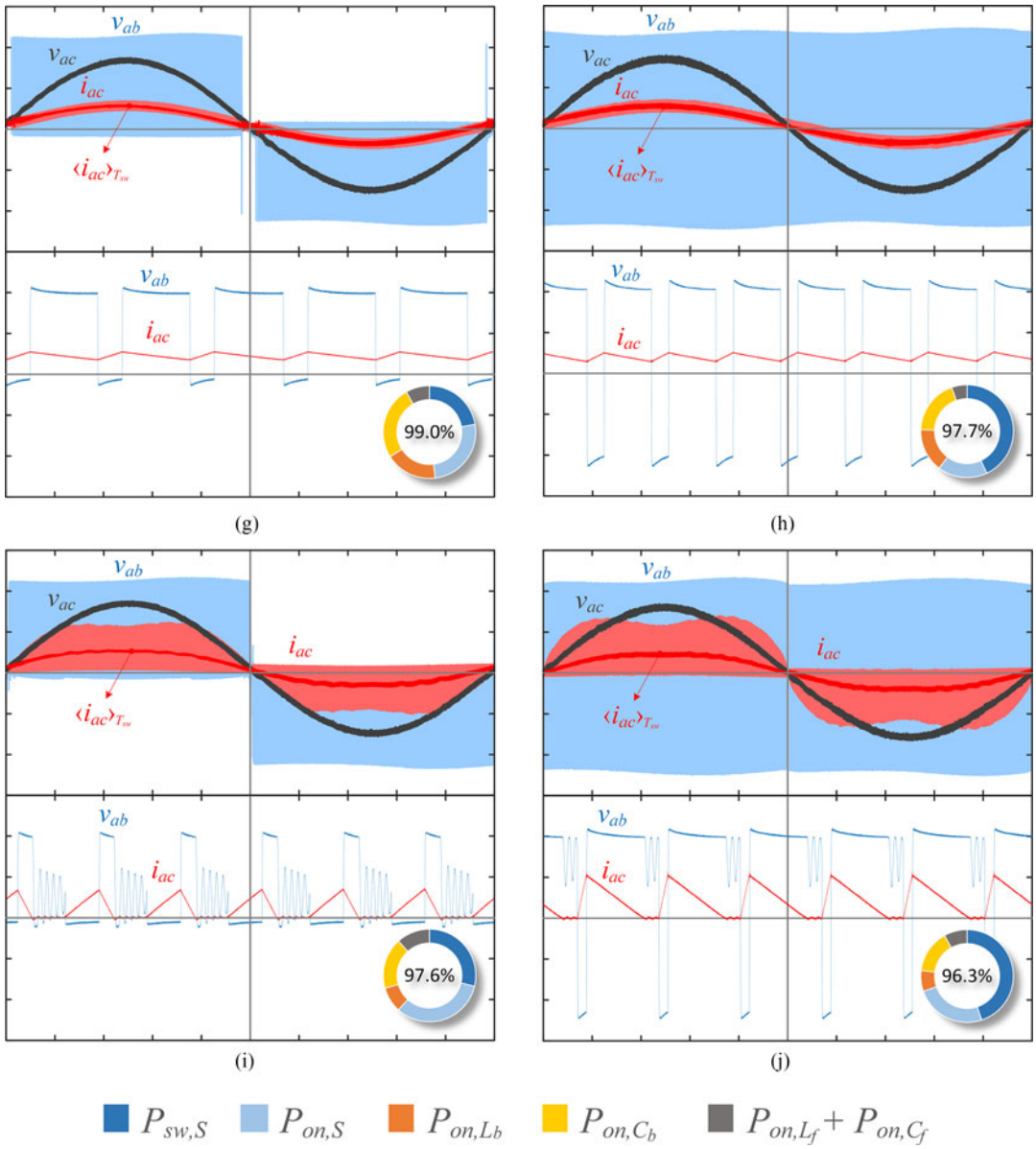

Fig. 10. continue.

the measured efficiency and the simulated power loss distribution at maximum power, i.e., 3680 W, is shown in the lower right corner. In the power loss distribution the switching losses of switching devices, $P_{sw,S}$, the conduction losses of switching devices, $P_{on,S}$, the boost-inductor losses, P_{on,L_b}, the bus capacitor losses, P_{on,C_b}, and the filter losses, $P_{on,L_f} + P_{on,C_f}$, have been taken into account.

The fixed frequency strategies operate at 60 kHz, whereas the variable frequency strategies work between 35 and 150 kHz. For all ZVS strategies, a 26-μH boost inductance and 215-μH filter inductance have been used, as well as a 215-μH boost inductance and 50-μH filter inductance for all hard switching strategies.

As it can be seen, the zero-cross distortion appears when the half-bridge configurations are used, whereas is avoided with the full-bridge configurations. On the other hand, the boost current ripple increases what supposes more conduction losses and switching losses in switching devices since the turn-OFF switching current is higher. For these reasons, the efficiency decreases lightly. The DCM operation mode, however, avoids the zero-cross distortion with the half-bridge configuration. Consequently, the full-bridge and hybrid configuration are less interesting in this case. With this operation mode, a small oscillation of the current is appreciated due to the diode parasitic capacity along with the boost coil.

The variable frequency strategies using hybrid configuration have been implemented too. Fig. 11 shows the main experimental waveforms. In both cases, ZVS and hard switching strategy, the zero-cross distortion is avoided because the full-bridge configuration is used when the absolute value of the mains voltage is lower than 100 V. The zoomed details show the moment this change is performed.

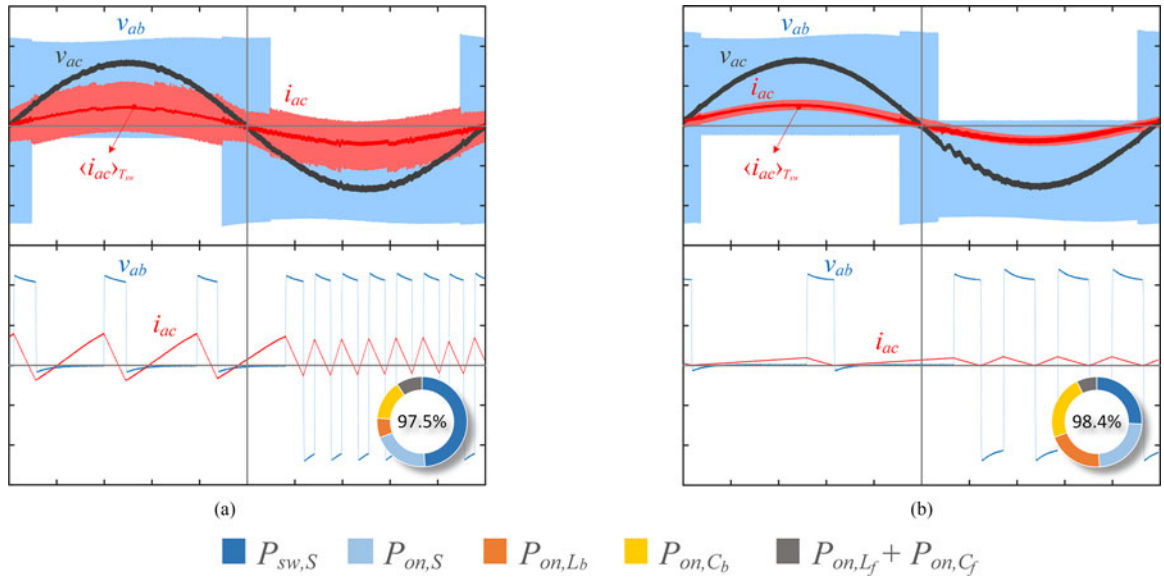

Fig. 11. ZVS (a) and hard switching (b) hybrid variable frequency CCM modulation strategies. On the top, the main experimental waveforms (voltage: 200 V/div, current: 50 A/div, and time: 2 ms/div) and, on the bottom, a zoomed detail of the moment of the change (time: 10 μs/div). In the lower right corner, the overall efficiency and the power loss distribution at maximum power, 3680 W.

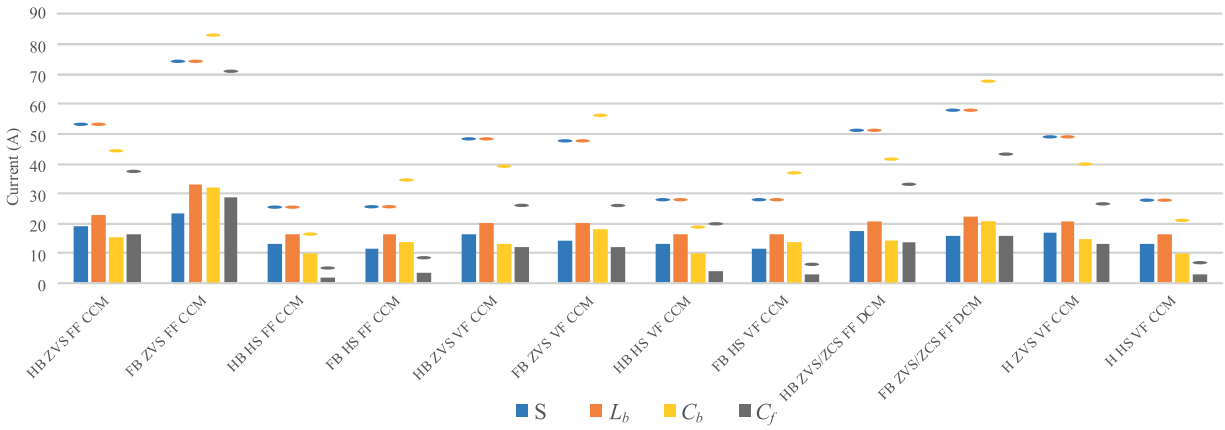

Fig. 12. Peak current, I_p, and the RMS current, I_{RMS}, of the switching devices, S, of the boost inductance, L_b, of the bus capacitor, C_b, and of the filter capacitor, C_f, at maximum power, 3680 W, according to the modulation strategy.

B. Comparative Analysis and Discussion

This section provides a comparative analysis and discussion of the proposed modulation strategies. The advantages and disadvantages have been analyzed, taking into account several parameters: device stress, efficiency, power loss distribution, operating frequency, control complexity, and EMC issues. This discussion allows us finding the modulation strategy better suited according to the implementation requirements and the application area.

1) Device Stress: The current ratings of the converter components depend on the implemented modulation strategy. The bar chart of Fig. 12 depicts the peak current, I_p, and the RMS current, I_{RMS}, of the switching devices, S, of the boost inductance, L_b, of the bus capacitor, C_b, and of the filter capacitor, C_f, at maximum power, 3680 W, according to the modulation strategy.

The maximum voltage applied over the switching devices just depends on the bus voltage, v_b, i.e., 400 V. The average current, 4.5 A approximately, just depends on the output power and the bus voltage, therefore, is independent of the modulation strategy. Taking into account the average current in both branches, 9 A, and the bus voltage, 400 V, an output power of 3680 W is obtained. The worst cases of RMS current and peak current are found in the ZVS CCM and DCM strategies due to the high ripple of the current. With 75-A peak current and 23-A RMS current, the full-bridge fixed frequency strategy stands out among them. The hard switching CCM strategies are the best cases. All of them are very similar. With 11.5-A RMS current and 25-A peak current the full-bridge fixed frequency strategy gets the lowest ratings. Finally, another point to consider is that using full-bridge configuration the RMS current is evenly distributed in each switching device whereas using half bridge

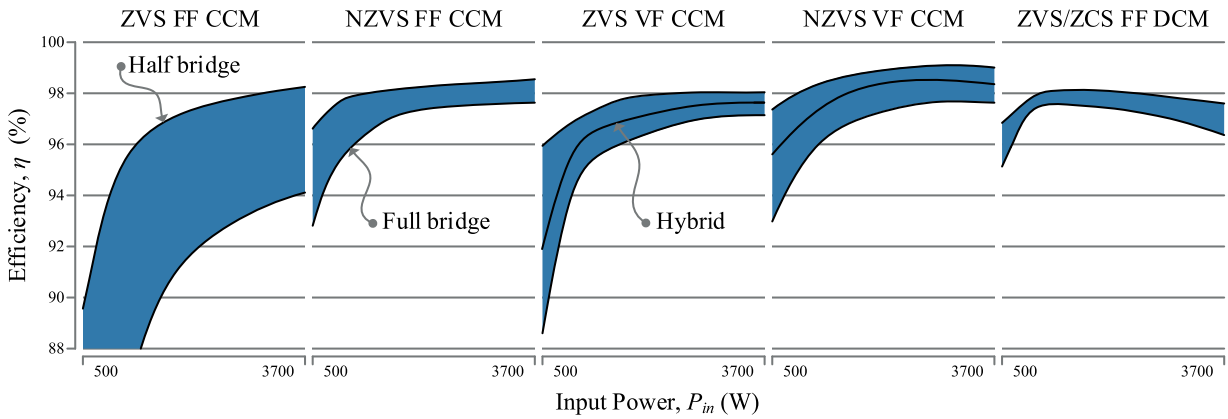

Fig. 13. Overall efficiency, η, as a function of the input power for each modulation strategy. The upper border using half-bridge configuration and the lower border using full-bridge configuration. Between the upper and the lower border the hybrid configuration as a function of the change voltage. In black line the hybrid ZVS and hard switching variable frequency CCM modulation strategy with 100-V change voltage.

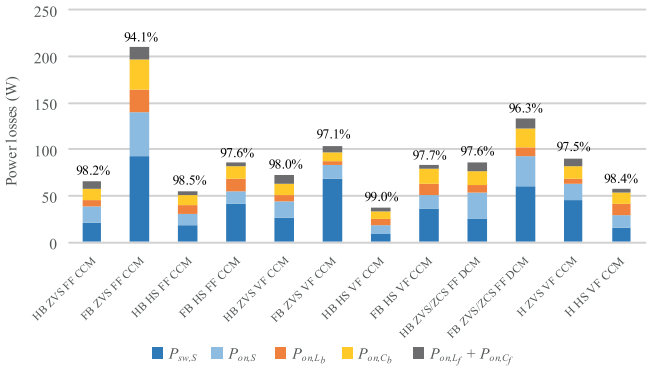

Fig. 14. Power loss distribution and experimental overall efficiency at maximum power, 3680 W, according to the modulation strategy.

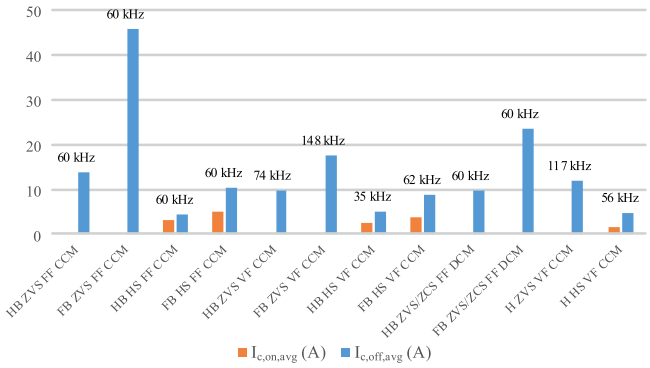

Fig. 15. Turn-OFF and turn-ON average switching current at maximum power, 3680 W according to the modulation strategy. The operating frequency is shown above each bar (average frequency considered for variable frequency strategies).

not. In this configuration, the worst case has been taken into account.

The maximum voltage applied over the boost inductance depends on the configuration topology so that using half-bridge configuration this voltage is v_b, i.e., 400 V, whereas using full-bridge configuration is $v_b + v_{ac}$, i.e., 725 V, or using hybrid configuration is $v_b + v_{th}$, i.e., 500 V. Therefore, the insulation requirements of the boost inductance are lower using half-bridge

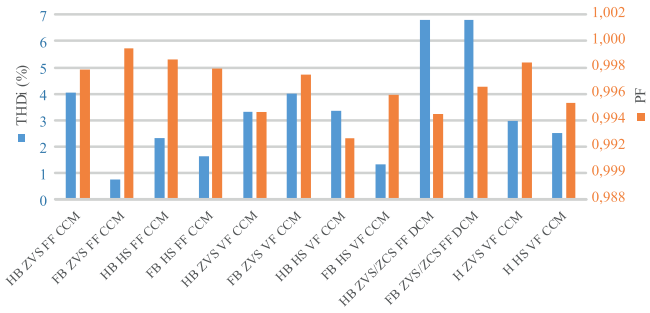

Fig. 16. THD of the mains current, $\mathrm{THD_i}$, and PF at maximum power, 3680 W, according to the modulation strategy.

configuration. The average current, 14.4 A, just depends on the input current, 16 A, or the input power, 3680 W. The peak currents are the same that in the switching devices whereas the RMS currents are higher. The full-bridge ZVS fixed frequency is the worst case with 75-A peak current and 33-A RMS current. The half-bridge hard switching fixed frequency is the best case with 25-A peak current and 16.1-A RMS current.

The maximum voltage applied over the bus capacitor is the bus voltage, v_b, i.e., 400 V. The modulation strategies that get the worst and the best current rating are the same as before with 83-A peak current and 31.7-A RMS current, and 16-A peak current and 9.7-A RMS current, respectively.

Finally, the maximum voltage over the filter inductance and capacitance is the mains voltage, i.e., 325 V. The current ratings of the filter inductance are the mains current ratings, i.e., 23-A peak current and 16-A RMS current whereas the current rating of the filter capacitor are given by the bar chart of Fig. 12 according to the modulation strategy.

2) Efficiency and Power Loss Distribution: The efficiency is measured using a power analyzer. The results as a function of the input power are shown in the graphs of Fig. 13. Using the half-bridge hard switching variable frequency CCM, the efficiency reaches up to 99% around the maximum power, i.e., 3680 W, surpassing the rest of modulation strategies in the whole operating range. However, the full-bridge ZVS fixed frequency CCM gets the worst efficiency, reaching just up to 94% at maximum

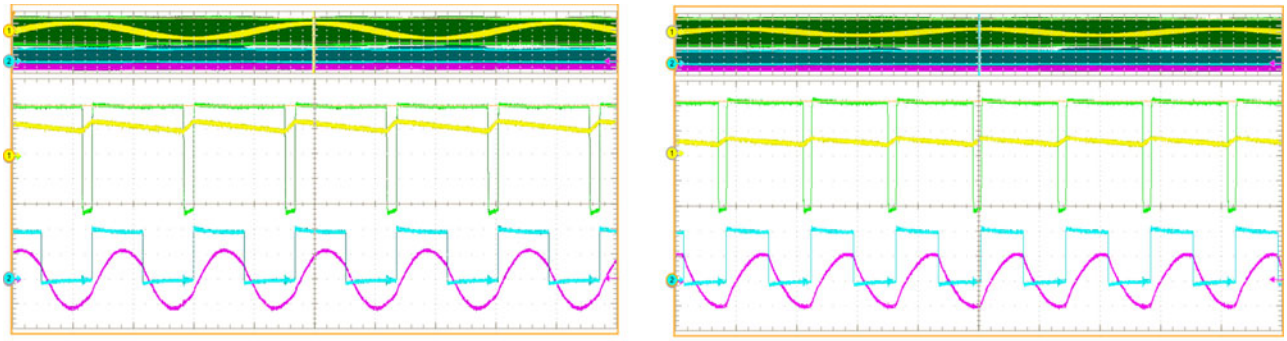

Fig. 17. Main waveforms of the PFC IH converter at maximum power, 3680 W, (a) and 1500 W of power (b). From top to bottom: voltage between a and b branches, v_{ab}, (200 V/div, green), boost inductance current, i_{ac}, (20 A/div, yellow), output voltage, v_o, (200 V/div, blue), and output current, i_o, (30 A/div, purple). Time: 10 μs/div.

power. As shown in Fig. 10(b), it is due to the high ripple of the current in the zero crossing to work at the same frequency. Besides, a similar ripple is necessary to work at the same frequency at lower powers. Since the conduction and switching losses are similar, the efficiency is further penalized at low power. An option to improve this result consists in changing the operating frequency as a function of the power in order to get ZVS with a properly current ripple. This approach is interesting using an inductive IH load. In this case, the PFC stage and the IH-inverter are synchronized at the same frequency. The output power is controlled by modifying the operating frequency. When the frequency is increased, the current ripple in the PFC stage is lower, decreasing switching, and conduction losses.

The efficiency of the implemented hybrid strategies is shown in black line in graphs of Fig. 13. With a 100-V change voltage, v_{th}, this parameter is improved a 1% approximately at maximum power in comparison with the full-bridge configuration. In this way, the zero-cross distortion using half-bridge configuration is avoided.

Fig. 14 shows the power loss distribution and efficiency at maximum power. Using the ZVS CCM and DCM modulation strategies, the ripple current is higher. It can be appreciated that this affects to the conduction losses of the converter components. Moreover, with full-bridge configuration the switching losses are higher due to the fact that the number of switching devices is increased.

Fig. 15 shows the turn-OFF and turn-ON average switching current according to the modulation strategy. This parameter along with the operating frequency and the switching energy of the MOSFETs allows us approximating the turn-ON and turn-OFF losses. In ZVS CCM and DCM strategies, there are not turn-ON switching losses, therefore, the turn-ON average current has not been taken into account. The turn-ON switching energy of the MOSFETs is higher than the turn-OFF one. However, in hard switching modulation strategies the turn-OFF switching current is quite lower than in ZVS modulation strategies. Besides, the turn-ON current is also low. For these reasons, the switching losses are usually higher in ZVS CCM and DCM modulation strategies.

3) Operating Frequency and Control: On the one hand, there are application areas in which getting a fixed operating frequency along the mains cycle is important. For example, in domestic IH-converters, modulating with different inverters at different working frequencies can produce acoustic noise. In these cases, working with fixed frequency modulation strategies is essential to get a proper operation. On the other hand, working with variable frequency modulations allows us distributing the harmonic currents in a wide frequency range, decreasing the EMC issues.

The control complexity and cost have been also analyzed. First, all control strategies have to measure the mains voltage to synchronize with the mains. The fixed-frequency activation control strategy is the least expensive control strategy because it just needs to measure the bus voltage. After this, the easiest control strategy is the boost-inductor voltage control, since it just has to measure the mains current, or the variable-frequency activation control using half-bridge configuration, because it just needs to measure the zero crossing of the boost inductance current. Finally, the most expensive strategies are the variable-frequency activation control using full-bridge or hybrid configuration, because it also needs to measure the bus voltage as well as the zero crossing of the boost inductance current, or the current mode control, since it must measure the boost inductance current. The boost inductance current measure is more expensive than mains current measure because the current sensor needs more requirements such as a higher sampling frequency.

4) Electromagnetic Compatibility (EMC): Fig. 16 depicts the total harmonic distortion of the current, $\mathrm{THD_i}$, and the power factor, PF, of the implemented modulation strategies. It can be appreciated that all strategies reach a PF greater than 0.99. Moreover, the $\mathrm{THD_i}$ is less than 4%, getting a sinusoidal current waveform. The $\mathrm{THD_i}$ of DCM modulation strategies reaches up to the 6.8% due to the current waveform is distorted. This distortion is produced because the boost inductance equivalent series resistance (ESR) and the diode reverse current have not been taken into account in the fixed-frequency activation control strategy. This issue can be solved using a correction factor or an outer control loop.

C. Domestic IH Application

Finally, the proposed converter has been used to power an IH-load with a 5-Ω equivalent series resistance, R_{eq}, and

80-μH equivalent series inductance, $L_{\rm eq}$. A 170 − nF resonant capacitor has been placed in order to obtain a 45-kHz resonant frequency.

According to the analysis performed, the full-bridge hard-switching fixed-frequency CCM modulation strategy gets a good tradeoff between efficiency, device stress, implementation and control cost, and EMC. Besides, it avoids the zero-cross distortion and the acoustic noise, since it works at a fixed frequency synchronized with the IH-inverter. For this reason, it has been selected for performing this application.

Fig. 17 depicts the experimental measurements with the converter operating at 60 kHz at maximum power and 71 kHz at 1500 W, where the main waveforms of the PFC and the IH-load are shown.

V. Conclusion

In this paper, the use of active PFC rectifiers has been proposed to increase the power and the performance of domestic induction heating appliances. For this purpose, a boost-type topology has been presented and every modulation strategy has been proposed.

The modulation strategies have been classified depending on the topology configuration (full bridge or half bridge) and the operation mode (CCM or DCM). Besides, the switching mode, ZVS or hard switching, and the operating frequency, fixed or variable, have been taken into account. The advantages and disadvantages of each one have been analyzed. Overall, in CCM the full-bridge topology avoids the zero-cross distortion at the cost of less efficiency, however, in DCM this distortion does not exist using half-bridge configuration. The use of hybrid strategies has been proposed to get a good balance between zero-cross distortion and efficiency.

In order to implement the proposed modulation strategies, four control strategies have been presented and analyzed: the boost-inductor voltage control, the variable or fixed frequency activation control, and the current mode control.

Finally, the main experimental waveforms of the proposed modulation strategies using a 3.6-kW prototype has been depicted. A comparative analysis has been performed taking into account the device stress, the efficiency, the control complexity and the EMC issues. Moreover, a domestic IH application has been implemented using the full-bridge hard-switching fixed-frequency CCM modulation strategy getting a properly operation of the converter and proving the feasibility of this research.

References

[1] O. Lucía, P. Maussion, E. Dede, and J. M. Burdío, "Induction heating technology and its applications: Past developments, current technology, and future challenges," *IEEE Trans. Ind. Electron.*, vol. 61, no. 5, pp. 2509–2520, May 2014.

[2] O. Lucía, J. Acero, C. Carretero, and J. M. Burdío, "Induction heating appliances: Towards more flexible cooking surfaces," *IEEE Ind. Electron. Mag.*, vol. 7, no. 3, pp. 35–47, Sep. 2013.

[3] C. Bernal *et al.*, "Kochfeld mit einer Mehrzahl von Heizelementen," German Patent EP 3111723 A1, 2009.

[4] F. Forest, S. Faucher, J.-Y. Gaspard, D. Montloup, J.-J. Huselstein, and C. Joubert, "Frequency-synchronized resonant converters for the supply of multiwindings coils in induction cooking appliances," *IEEE Trans. Ind. Electron.*, vol. 54, no. 1, pp. 441–452, Feb. 2007.

[5] F. Forest, E. Labouré, F. Costa, and J.-Y. Gaspard, "Principle of a multi-load/single converter system for low power induction heating," *IEEE Trans. Ind. Electron.*, vol. 15, no. 2, pp. 223–230, Mar. 2000.

[6] O. Lucía, J. M. Burdío, L. A. Barragán, J. Acero, and C. Carretero, "Series resonant multi-inverter with discontinuous-mode control for improved light-load operation," *IEEE Trans. Ind. Electron.*, vol. 58, no. 11, pp. 5163–5171, Nov. 2011.

[7] O. Lucía, J. M. Burdío, L. A. Barragán, J. Acero, and I. Millán, "Series-resonant multiinverter for multiple induction heaters," *IEEE Trans. Power Electron.*, vol. 24, no. 11, pp. 2860–2868, Nov. 2010.

[8] H. Pham, H. Fujita, K. Ozaki, and N. Uchida, "Phase angle control of high-frequency resonant currents in a multiple inverter system for zone-control induction heating," *IEEE Trans. Power Electron.*, vol. 26, no. 11, pp. 3357–3366, Nov. 2011.

[9] T. Friedli, M. Hartmann, and J. W. Kolar, "The essence of three-phase PFC rectifier systems - Part II," *IEEE Trans. Power Electron.*, vol. 29, no. 2, pp. 543–560, Feb. 2014.

[10] J. W. Kolar and T. Friedli, "The essence of three-phase PFC rectifier systems - Part I," *IEEE Trans. Power Electron.*, vol. 28, no. 1, pp. 176–198, Jan. 2013.

[11] *Electromagnetic Compatibility (EMC) - Part 3-2: Limits - Limits for Harmonic Current Emissions (Equipment Input Current $<=$ 16 A per Phase)*, UNE-EN 61000-3-2:2014.

[12] Y. Kawaguchi *et al.*, "A comparison of operation mode for soft-switching PFC converter for induction heating cooking appliance," in *Proc. 35th Annu. Conf. IEEE Ind. Electron. Soc.*, 2009, pp. 13–18.

[13] Y. Kawaguchi *et al.*, "A comparative evaluation of DCM control and CCM control for soft-switching PFC converter," in *Proc. 36th Annu. Conf. IEEE Ind. Electron. Soc.*, 2010, pp. 250–255.

[14] M. M. Jovanovic and Y. Jang, "State-of-the-art, single-phase, active power-factor-correction techniques for high-power applications - An overview," *IEEE Trans. Ind. Electron.*, vol. 52, no. 3, pp. 701–708, Jun. 2005.

[15] J. Biela, D. Hassler, J. Miniböck, and J. W. Kolar, "Optimal design of a 5kW/dm³/ 98.3% efficient TCM resonant transition single-phase PFC rectifier," in *Proc. 2010 Int. Conf. Asia Power Electron.*, 2010, pp. 1709–1716.

[16] C. Marxgut, J. Biela, and J. W. Kolar, "Interleaved triangular current mode (TCM) resonant transition, single phase PFC rectifier with high efficiency and high power density," in *Proc. 2010 Int. Conf. Power Electron.*, 2010, pp. 1725–1732.

[17] C. Min and S. Jian, "Feedforward current control of boost single-phase PFC converters," *IEEE Trans. Power Electron.*, vol. 21, no. 2, pp. 338–345, Mar. 2006.

[18] Y. Jang and M. M. Jovanovic, "A bridgeless PFC boost rectifier with optimized magnetic utilization," *IEEE Trans. Power Electron.*, vol. 24, no. 1, pp. 85–93, Jan. 2009.

[19] C. Marxgut, F. Krismer, D. Bortis, and J. W. Kolar, "Ultraflat interleaved triangular current mode (TCM) single-phase PFC rectifier," *IEEE Trans. Power Electron.*, vol. 29, no. 2, pp. 873–882, Feb. 2014.

[20] M. S. Ortmann, T. B. Soeiro, and M. L. Heldwein, "High switches utilization single-phase PWM boost-type PFC rectifier topologies multiplying the switching frequency," *IEEE Trans. Power Electron.*, vol. 29, no. 11, pp. 5749–5760, Nov. 2014.

[21] N. Haryani, R. Burgos, and D. Boroyevich, "Variable frequency and constant frequency modulation techniques for GaN based MHz H-bridge PFC," in *Proc. 2015 Int. Conf. IEEE Appl. Power Electron.*, 2015, pp. 1889–1896.

[22] F. Jauch and J. Biela, "Combined phase-shift and frequency modulation of a dual-active-bridge AC–DC converter with PFC," *IEEE Trans. Power Electron.*, vol. 31, no. 12, pp. 8387–8397, Dec. 2016.

[23] J. H. Park, D. J. Kim, and K. B. Lee, "Predictive control algorithm including conduction-mode detection for PFC converter," *IEEE Trans. Ind. Electron.*, vol. 63, no. 9, pp. 5900–5911, Sep. 2016.

Mario Pérez-Tarragona (S'15) received the M.Sc. degree in electrical engineering from the University of Zaragoza, Zaragoza, Spain, in 2015, where he is currently working toward the Ph.D. degree in electronic engineering and comunications.

His researh interests include resonant PFC converters, resonant converters and digital control for induction heating applications.

Mr. Pérez-Tarragona is a member of the Aragon Institute for Engineering Research.

Héctor Sarnago (S'09–M'15) received the M.Sc. degree in electrical engineering and the Ph.D. degree in power electronics from the University of Zaragoza, Zaragoza, Spain, in 2010 and 2013, respectively.

He is currently a Senior Postdoctoral Researcher in the Department of Electronic Engineering and Communications, University of Zaragoza. His main research interests include resonant converters and digital control for induction heating applications.

Mr. Sarnago is a member of the Aragon Institute for Engineering Research.

Óscar Lucía (S'04–M'11–SM'14) received the M.Sc. and Ph.D. degrees (Hons.) in electrical engineering from the University of Zaragoza, Zaragoza, Spain, in 2006 and 2010, respectively.

During 2006 and 2007, he held a research internship at the Bosch and Siemens Home Appliances Group. Since 2008, he has been with the Department of Electronic Engineering and Communications, University of Zaragoza, where he is currently an Associate Professor. During part of 2009 and 2012, he was a Visiting Scholar at the Center of Power Electronics Systems, Virginia Tech. His main research interests include resonant power conversion, wide-bandgap devices, and digital control, mainly applied to contactless energy transfer, induction heating, electric vehicles, and biomedical applications. In these topics, he has published more than 50 international journal papers and 125 conference papers, and he has filed more than 25 patents.

Dr. Lucía is an active member of the Power Electronics and Industrial Electronics Societies. He was a Guest Associate Editor of the IEEE TRANSACTIONS ON INDUSTRIAL ELECTRONICS and the IEEE JOURNAL OF EMERGING AND SELECTED TOPICS IN POWER ELECTRONICS in 2013 and 2015, respectively. He is currently an Associate Editor of the IEEE TRANSACTIONS ON INDUSTRIAL ELECTRONICS and the IEEE TRANSACTIONS ON POWER ELECTRONICS. He is a member of the Aragon Institute for Engineering Research.

José M. Burdío (M'97–SM'12) received the M.Sc. and Ph.D. degrees in electrical engineering from the University of Zaragoza, Zaragoza, Spain, in 1991 and 1995, respectively.

He has been with the Department of Electronic Engineering and Communications, University of Zaragoza, where he is currently a Professor, the Head of the Group of Power Electronics and Microelectronics, and the Director of the BSH Power Electronics Laboratory. During 2000, he was a Visiting Professor at the Center for Power Electronics Systems, Virginia Tech. He is the author of more than 80 international journal papers and over 200 papers in conference proceedings and the holder of more than 60 international patents. His main research interests include modeling of switching converters and resonant power conversion for induction heating and biomedical applications.

Dr. Burdío is a senior member the Power Electronics and Industrial Electronics Societies. He is also a member of the Aragon Institute for Engineering Research.